







Escherichia coli limits Salmonella Typhimurium infections after diet shifts and fat-mediated microbiota perturbation in mice

Other Journal Item

Author(s):

Wotzka, Sandra Y.; Kreuzer, Markus; Maier, Lisa; Arnoldini, Markus; Nguyen, Bidong D.; Brachmann, Alexander O.; Berthold, Dorothée L.; [Zünd, Mirjam](#) ; Hausmann, Annika; Bakkeren, Erik; [Hoces Burga, Daniel Alexander](#) ; Gül, Ersin; Beutler, Markus; Dolowschiak, Tamas; Zimmermann, Michael; Fuhrer, Tobias; Moor, Kathrin; [Sauer, Uwe](#) ; Typas, Athanasios; Piel, Jörn; Diard, Médéric; Macpherson, Andrew J.; Stecher, Bärbel; [Sunagawa, Shinichi](#) ; [Slack, Emma](#) ; [Hardt, Wolf-Dietrich](#) 

Publication date:

2019-12

Permanent link:

<https://doi.org/https://doi.org/10.3929/ethz-b-000382128>

Rights / license:

[In Copyright - Non-Commercial Use Permitted](#)

Originally published in:

Nature Microbiology 4(12), <https://doi.org/10.1038/s41564-019-0568-5>

Funding acknowledgement:

- Deciphering the initial steps of Salmonella diarrhea in vivo. ()
- Deciphering the initial steps that lead to Salmonella Typhimurium diarrhea ()

Escherichia coli limits *Salmonella* Typhimurium infections after diet shifts and fat-mediated microbiota perturbation in mice

Sandra Y. Wotzka^{1,7}, Markus Kreuzer^{1,7}, Lisa Maier², Markus Arnoldini¹, Bidong D. Nguyen¹, Alexander O. Brachmann¹, Dorothee L. Berthold¹, Mirjam Zünd¹, Annika Hausmann¹, Erik Bakkeren¹, Daniel Hoces¹, Ersin Gül¹, Markus Beutler³, Tamas Dolowschiak¹, Michael Zimmermann⁴, Tobias Fuhrer⁴, Kathrin Moor¹, Uwe Sauer⁴, Athanasios Typas², Jörn Piel¹, Médéric Diard¹, Andrew J. Macpherson⁵, Bärbel Stecher^{3,6}, Shinichi Sunagawa¹, Emma Slack¹ and Wolf-Dietrich Hardt^{1*}

The microbiota confers colonization resistance, which blocks *Salmonella* gut colonization¹. As diet affects microbiota composition, we studied whether food composition shifts enhance susceptibility to infection. Shifting mice to diets with reduced fibre or elevated fat content for 24 h boosted *Salmonella* Typhimurium or *Escherichia coli* gut colonization and plasmid transfer. Here, we studied the effect of dietary fat. Colonization resistance was restored within 48 h of return to maintenance diet. *Salmonella* gut colonization was also boosted by two oral doses of oleic acid or bile salts. These pathogen blooms required *Salmonella*'s AcrAB/TolC-dependent bile resistance. Our data indicate that fat-elicited bile promoted *Salmonella* gut colonization. Both *E. coli* and *Salmonella* show much higher bile resistance than the microbiota. Correspondingly, competitive *E. coli* can be protective in the fat-challenged gut. Diet shifts and fat-elicited bile promote *S. Typhimurium* gut infections in mice lacking *E. coli* in their microbiota. This mouse model may be useful for studying pathogen-microbiota-host interactions, the protective effect of *E. coli*, to analyse the spread of resistance plasmids and assess the impact of food components on the infection process.

We hypothesized that shifts in diet composition might affect colonization resistance, as 24–48 h on diets with elevated fat or reduced fibre content suffice to alter microbiota compositions, and fibre deprivation accelerates murine *Citrobacter rodentium* infections^{2,3}. We initially analysed a typical high-fat Western-type diet without fibre (WD; Fig. 1a). C57BL/6 mice harbouring an unperturbed, complex, *E. coli*-free microbiota (CON^E; Supplementary Table 1) were reared on a standard plant-based maintenance diet (MD). Mice remaining on MD had limited gut luminal *Salmonella* Typhimurium (*S.Tm*) strain SL1344 growth (Fig. 1b). In spite of possible batch-to-batch variations, this colonization resistance has been consistent over many years⁴. Another group was shifted to WD 24 h before per-oral inoculation with *S.Tm* (Fig. 1a–d). Strikingly, this group featured 10²–10⁵-fold higher stool pathogen loads than the MD controls (Fig. 1b). Stool pathogen loads rose almost as quickly

as in antibiotic pre-treated animals⁴. Also, WD-shifted mice showed elevated gut luminal pathogen loads, exacerbated systemic infection and increased enteropathy by 96 h post infection (p.i.) (Fig. 1c,d). Shifts to WD also promoted *S.Tm* gut colonization in C57BL/6 mice carrying a defined *Escherichia coli*-free consortium (Oligo-MM¹² (ref. 5)), C57BL/6 mice carrying another complex microbiota (CON^R, includes *E. coli*) and 129SvEv mice (CON^X microbiota, no *E. coli*; Supplementary Fig. 2a–d and Supplementary Table 1). Furthermore, WD-shifts boosted gut colonization by a second wild-type (WT) *S.Tm* strain (ATCC14028; Supplementary Fig. 6), the mouse commensal *E. coli* 8178 (ref. 6) (Supplementary Fig. 2e) and by *S.Tm*^{avir}, an avirulent *S.Tm* mutant (Supplementary Fig. 3 and Supplementary Table 2), which grows luminally without eliciting enteropathy. *S.Tm* blooms were also observed after shifts to a fibre-containing high-fat diet, but not the low-fat control (Supplementary Fig. 4). Thus, fat might be involved. As a fibre-free low-fat diet also enhanced *S.Tm* colonization (Supplementary Fig. 4), we conclude that gut luminal growth of *S.Tm* and other Enterobacteriaceae is promoted not only by fibre deprivation, as reported previously³, but also by fat and possibly other unidentified food constituents.

We decided to focus on the role of fat, as associated microbiota changes and disease phenotypes hinted at this nutrient being one possible trigger of Enterobacteriaceal blooms^{2,7–9}. First, we supplemented MD with additional lard. Shifts to this diet promoted *S.Tm* gut colonization (Supplementary Fig. 2f). We then gavaged mice on MD with oleic acid. This unsaturated fatty acid does not elicit inflammatory responses¹⁰ and is a main digestive breakdown product of lard (~45%). In mice on MD, oleic acid doses of as little as ~0.4 ml per kg bodyweight raised pathogen stool loads by tenfold ($P < 0.05$; $2 \times 10 \mu\text{l}$; Supplementary Fig. 5). This corresponds to doses of ~60 g of animal fat for a 70 kg person. Human high-fat diets can include >150 g fat per day. Doses of $>2 \times 10 \mu\text{l}$ oleic acid boosted gut luminal *S.Tm* colonization by 10⁴-fold and significantly aggravated *S.Tm*-inflicted disease (Fig. 1a–d, Supplementary Figs. 2a,b and 5). Thus, short exposures to fat or oleic acid can promote *S.Tm* blooms, at least in *E. coli*-free mice.

¹Institute of Microbiology, D-BIOL, ETH Zürich, Zürich, Switzerland. ²European Molecular Biology Laboratory, Heidelberg, Heidelberg, Germany.

³Max von Pettenkofer Institute, Faculty of Medicine, LMU Munich, Munich, Germany. ⁴Institute of Molecular Systems Biology, D-BIOL, ETH Zürich, Zürich, Switzerland. ⁵Maurice Müller Laboratories, University Clinic for Visceral Surgery and Medicine, University of Bern, Bern, Switzerland. ⁶German Center for Infection Research (DZIF), Munich, Germany. ⁷These authors contributed equally: Sandra Y. Wotzka, Markus Kreuzer. *e-mail: hardt@micro.biol.ethz.ch

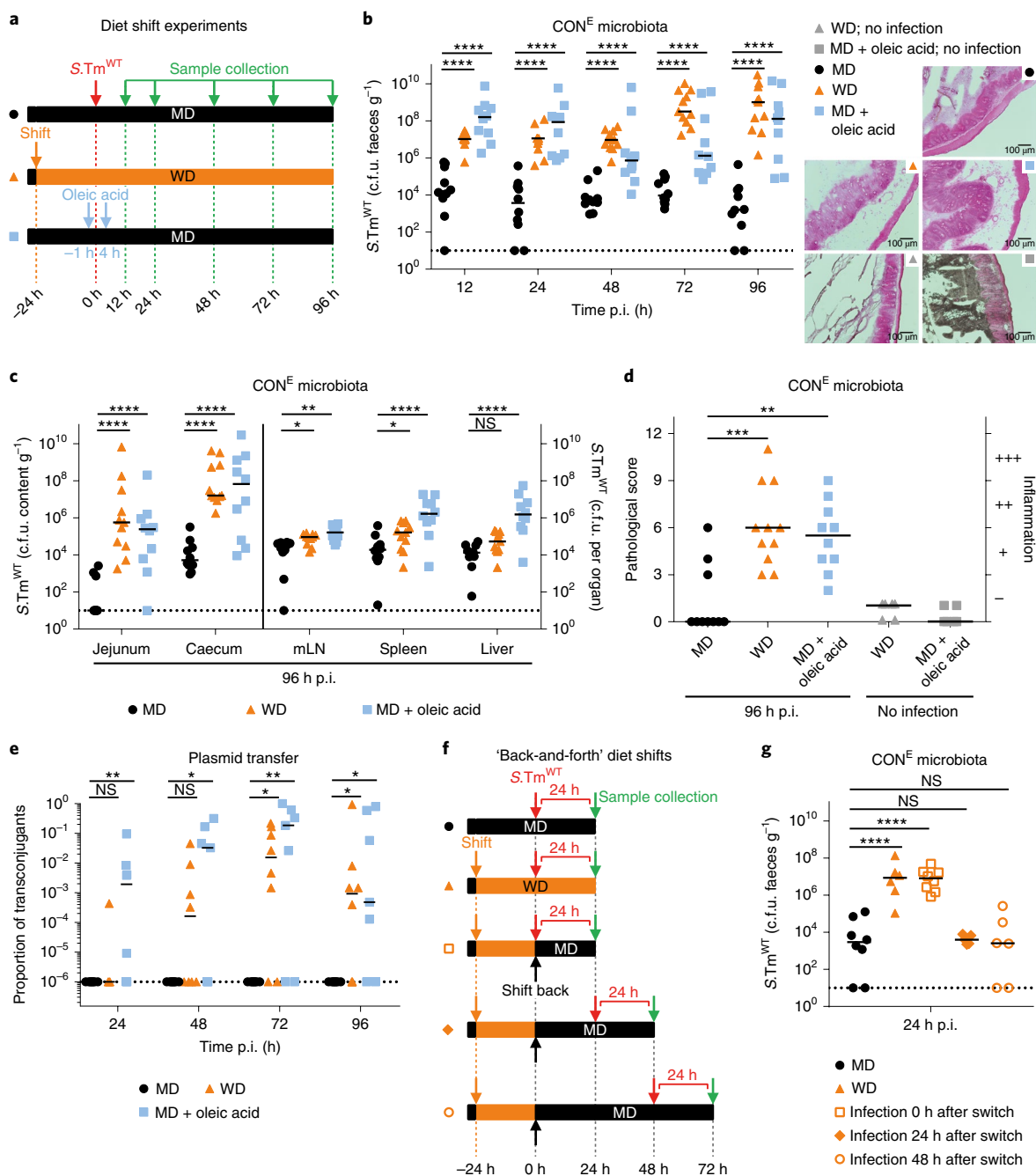


Fig. 1 | A shift to WD and oleic acid gavage promote *S.Tm* blooms, enteropathy and plasmid transfer. **a**, Experimental protocol. **b–d**, Pathogen loads and caecum tissue histopathology of CON^E mice infected with 5×10^7 colony-forming units (c.f.u.) *S.Tm* by gavage ($n = 6, 10$ and 11). Non-infected controls 96 h after diet shift or oleic acid gavage are shown as grey symbols ($n = 6$; no c.f.u. detected). See ‘Histological procedures’ in Methods for details of pathological scoring. Haematoxylin and eosin (H&E) images represent a median sample from the corresponding treatments. **e**, In vivo transconjugation was determined by stool plating ($n = 7, 8$; Kruskal–Wallis test, multiple comparison correction; Supplementary Fig. 6). **f**, Protocol of back-and-forth diet shifts in CON^E mice. **g**, Faecal pathogen loads were analysed 24 h p.i. with 5×10^7 c.f.u. *S.Tm* (by gavage; $n = 5, 6, 8$ and 9 mice). Bars represent the median; two-way analysis of variance (ANOVA) on log-normalized data with Dunnett’s multiple comparison test (**b, c, g**); two-tailed Mann–Whitney U-test (**d**). Dotted lines indicate detection limits. NS, not significant ($P > 0.05$); * $P < 0.05$, ** $P < 0.01$, *** $P < 0.005$, **** $P < 0.001$. MD, maintenance diet; WD, Western-type diet; mLN, mesenteric lymph node.

Dysbiosis-mediated Enterobacteriaceae blooms can fuel the spread of resistance plasmids¹¹. To test if WD-shift or oleic acid-promoted blooms have a similar effect, we studied transfer rates of plasmid PII from *S.Tm* SL1344 (that is, PII^{CMR} carrying chloramphenicol resistance). PII belongs to an IncII-family of antibiotic-resistant and colicin plasmids commonly found in Enterobacteriaceae⁶.

Mice were sequentially infected with the recipient strain (*S.Tm* ATCC14028^{KmR}) and 15 min later with the donor (*S.Tm* SL1344, PII^{CMR}). Indeed, WD-shift and oleic acid boosted plasmid transfer by 10^2 – 10^6 -fold compared to controls (Fig. 1e and Supplementary Fig. 6). It remains unclear if this is solely attributable to increased donor/recipient densities.

The microbiota composition changed 12–24 h after WD-shift or oleic acid gavage (Supplementary Fig. 7). This provided a hint that microbiota disturbance might explain the elevated susceptibility to *S.Tm*. The alleviation of colonization resistance was transient. After return to MD, the mice regained full colonization resistance within 24–44 h (Fig. 1g and Supplementary Fig. 8). Therefore, our subsequent mechanistic analysis focused on the time window of 0–24 h after the dietary perturbation.

Next, we tested if bile salts might be involved. Fat digestion necessitates bile salt release into the gut lumen^{12,13}. Although most bile is resorbed before passage into the large intestine, faecal concentrations can reach ~0.3% (w/v) after fat consumption¹⁴. Indeed, bile salts were elevated in the caecal contents after the WD-shift or oleic acid gavage (Supplementary Fig. 9). Cholate, a primary bile salt, reached concentrations of up to 0.1% (Fig. 2a). These data hinted at bile salt-mediated alleviation of colonization resistance, as bile salts are well-known inhibitors for numerous bacterial species^{15,16}, but not *Salmonella* or *E. coli* spp.¹⁷. This has been utilized in stool diagnostics, which traditionally employs bile supplements to culture *Salmonella* or *E. coli* spp. while suppressing unwanted microorganisms¹⁸. To establish the role of bile salts in alleviating colonization resistance, we administered cholate by oral gavage at 1 h before and 4 h after infection. Two doses of cholate (100 μ l, 8%) promoted *S.Tm* gut colonization almost as efficiently as streptomycin (streptomycin *S.Tm* enterocolitis model⁴; Fig. 2b,c), while gut transit times remained unaltered (Supplementary Fig. 10). Taurocholate, another primary bile salt, had a similar effect (Supplementary Fig. 11). Thus, bile salts alone can elicit *S.Tm* blooms independent of dietary fat.

The microbiota were more sensitive to bile salts than WT *S.Tm* or *E. coli*. This was established by live/dead-dye exclusion from cholate-exposed gut luminal bacteria (Fig. 2d) and by cholate inhibition of the anaerobic growth of 16 representative strains isolated from human and nine strains from murine stools (from Oligo-MM¹²-microbiota; Supplementary Table 3). Most microbiota strains were inhibited by $\geq 0.125\%$ cholate (Fig. 2e). In contrast, WT *S.Tm* and the human commensal *E. coli* ED1a were approximately tenfold more resistant than the microbiota or mutants lacking the AcrAB/TolC efflux pump, a known determinant of Enterobacteriaceae bile resistance^{19,20} (Fig. 2d,e and Supplementary Tables 2, 4 and 5). Equivalent observations were made with taurocholate (Supplementary Fig. 12). Thus, bile salts are sufficient to recapitulate the loss of colonization resistance associated with WD-shift or oleic acid treatment.

To assess, quantitatively, if bile-inflicted differences in growth rates are sufficient to explain why fat promotes *S.Tm* blooms, we formulated a mathematical model and used it to generate explicit predictions. Specifically, we modelled the outcome of competition (for colonizing the caecum lumen) between *S.Tm* and a generic microbiota after 24 h, using the bile salt-dependent growth parameters derived from Fig. 2e (see Supplementary Information on the model for details; Supplementary Table 6 and Supplementary Figs. 13–15). This recapitulated the behaviour of our system. WT *S.Tm* outcompeted the microbiota at bile salt concentrations realistic in the fat-exposed caecum, whereas the microbiota stayed dominant at bile salt concentrations below 0.15% (Fig. 3a). In contrast, an *acrAB* mutant could not efficiently outcompete the microbiota, even at high bile salt concentrations (*S.Tm*^{*acrAB*}; Fig. 3b). Thus, bile salt-mediated growth inhibition is sufficient to explain why WD, dietary fat and oleic acid promote gut infection.

This was verified by competitive infection experiments of WT *S.Tm* versus *acr* mutants that feature a similar bile salt sensitivity as most Bacteroidetes or Firmicutes strains (Fig. 2e). When WD-shift, oleic acid or cholate were applied (but not in the MD controls), WT *S.Tm* outcompeted the *acr* mutants (Fig. 3c,d and Supplementary Figs. 16 and 17). In keeping, *S.Tm*^{*acrAB*} yielded lower gut luminal densities than WT *S.Tm* after WD-shifts. To further assess the colonization defect of *S.Tm*^{*acrAB*}, we infected mice after WD-shifts with

one *S.Tm* strain at a time (Fig. 3e). These data establish bile resistance as a key factor promoting Enterobacteriaceae blooms in the fat-exposed gut.

Control experiments assessed if pathogen growth on fatty acids may fuel *S.Tm* blooms in the fat-exposed gut. However, caecal long-chain fatty acid (LCFA) concentrations remained unchanged after WD-shift or oleic acid gavage (Supplementary Fig. 18a,b). Moreover, *S.Tm*^{*fadL*}, which is deficient in LCFA uptake (Δ *fadL*), showed only a minor gut luminal growth attenuation (\leq twofold; Supplementary Fig. 18e). This defect was much smaller than the 10³- to 10⁴-fold growth difference of *S.Tm*^{WT} between WD- or oleic acid-exposed mice and animals on MD (Supplementary Fig. 18e). Similarly, we could exclude cross-feeding on products from other microbiota, like short-chain fatty acids (SCFAs; acetate, propionate, butyrate; Supplementary Fig. 18f–i). In conclusion, fatty acid utilization by *S.Tm* is not necessary for pathogen growth in the fat-exposed gut.

A second set of controls assessed if fat exposure might elicit gut inflammation and thereby enhance pathogen growth^{8,21–26}. However, within 24 h, neither WD-shift, nor gavage with oleic acid or cholate, affected cardinal mucosal inflammation marker expression, T_{reg} or phagocyte numbers implicated in disease-fueled *Salmonella* growth²⁶ (Supplementary Figs. 19–21). Thus, sub-acute inflammatory responses are dispensable for the alleviation of colonization resistance. Although interleukin-22 (IL-22) is dispensable in our model (Supplementary Fig. 22), it may contribute in other situations, as some animals featured elevated *il-22* and *reg-III β* , an antimicrobial peptide favouring Enterobacteriaceae blooms^{27–29} (Supplementary Fig. 19).

Further controls verified that expression of SPI-1, an inflammation-triggering virulence factor, was unaffected upon WD-shift or oleic acid gavage (Supplementary Fig. 23). Finally, competitive infections verified that nitrate respiration (as needed for *S.Tm* growth in the inflamed gut³⁰) was dispensable for accelerating growth in mice subjected to WD-shift or oleic acid (competitive index (CI) ≈ 1 ; Supplementary Fig. 24). Thus, mucosal inflammation is not required for fat-mediated promotion of *S.Tm* gut colonization (Supplementary Fig. 1, step 1b).

Finally, we assessed if *E. coli* may limit *S.Tm* infections after diet shifts. WT *E. coli* strains are common members of animal microbiota, encode AcrAB/TolC, are bile-resistant and bloom after WD-shift (Fig. 2e and Supplementary Figs. 2e and 12)^{31–33}. Moreover, some, but not all, *E. coli* strains are capable of outcompeting *Salmonella* spp. in the gut of mice and chickens^{6,34}. Correspondingly, *S.Tm* blooms were ~10- to 1,000-fold smaller when the microbiota includes a *Salmonella*-competitive *E. coli* (compare Fig. 1b versus Supplementary Fig. 2c; Supplementary Table 1). Therefore, competitive *E. coli* might limit fat-promoted pathogen blooms. CON^E mice were gavaged with oleic acid or shifted to WD as in Fig. 1a and co-infected with WT *S.Tm* and a mixture of three *E. coli* strains (5×10^7 c.f.u., by gavage; Supplementary Table 2 and Fig. 4a,b) capable of growth in 2% cholate. *E. coli* 8178 and CFT073 can outcompete *S.Tm* in antibiotic-treated mice⁶ and *E. coli* Z1324 is a recent isolate from a healthy human volunteer³³. Indeed, the *E. coli* mix colonized the murine gut, suppressed oleic acid- and WD-promoted *S.Tm* blooms by 10²- to 10⁵-fold and prevented enteropathy (Fig. 4a–c).

Within the *E. coli* mix, *E. coli* 8178 achieved the highest gut luminal densities. Indeed, *E. coli* 8178 alone could limit gut luminal *S.Tm* blooms after a WD-shift for 72–96 h. It did not matter whether *E. coli* 8178 was applied in parallel or 48 h before the *S.Tm* infection (Fig. 4d and Supplementary Fig. 25). However, *E. coli* 8178 alone was less efficient than the *E. coli* mix. We conclude that competitive *E. coli* can preserve colonization resistance after fat-mediated disturbance.

This work identifies fat as one factor promoting *Salmonella* diarrhoea in mice. Fat can achieve this by eliciting bile salts which

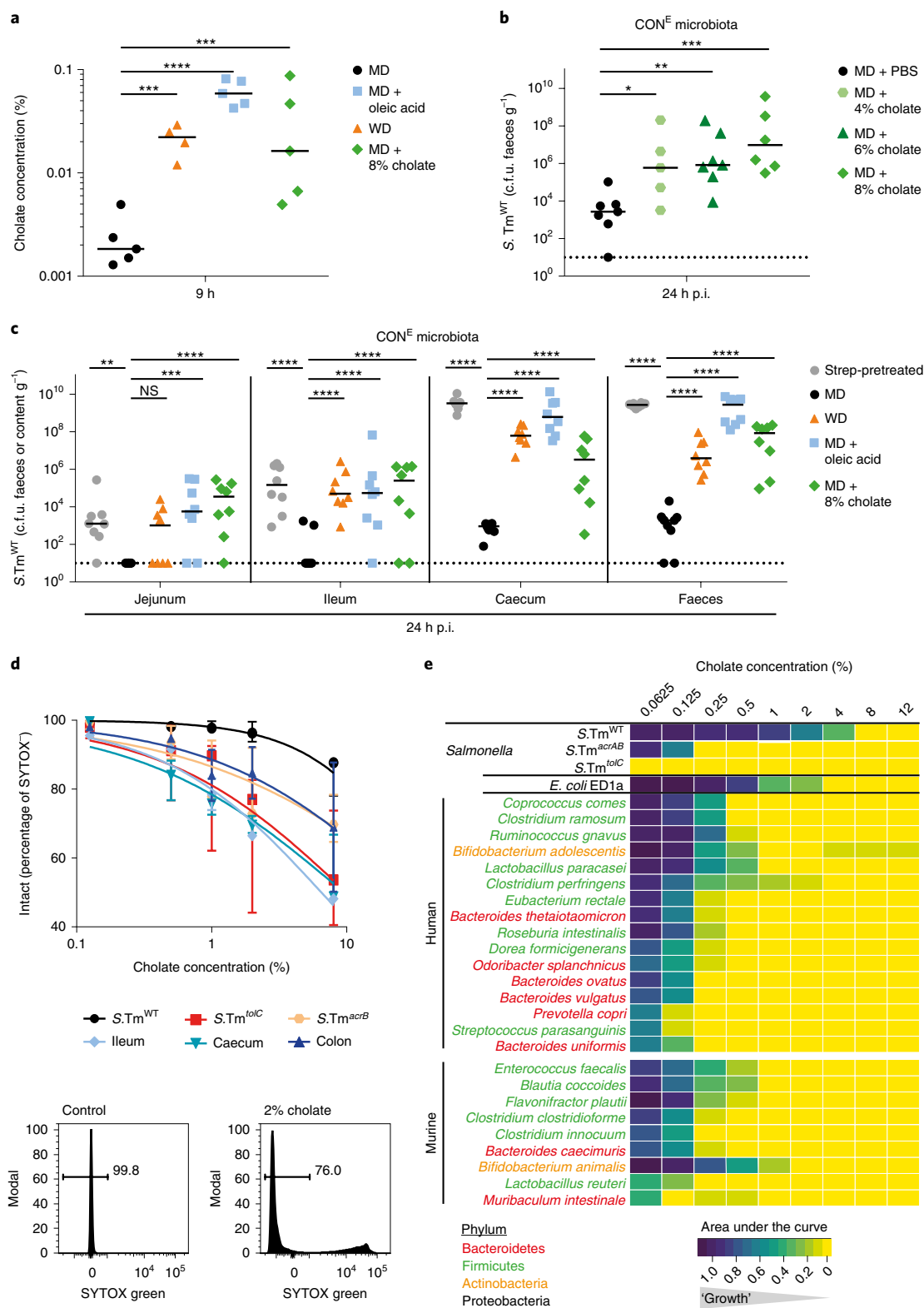


Fig. 2 | Primary bile salts can explain *S.Tm* blooms. **a**, Quantitative cholate mass spectrometry analysis in CON^E mice ($n=5$) 9 h after the indicated interventions. **b**, Cholate titration experiment. CON^E mice ($n=5, 6$ and 7) were gavaged, as indicated ($100\ \mu\text{l}$), 1 h before and 4 h after *S.Tm* infection (5×10^7 c.f.u.). **c**, Effect of the indicated interventions on gut luminal *S.Tm* densities ($n=8$ and 9). Control, CON^E mice pre-treated with streptomycin (20 mg by gavage; 24 h before infection; indicated by grey circles). **d**, Cholate sensitivity of gut luminal microbiota from ileum ($n=2$), caecum ($n=3$) and colon ($n=2$) microbiota (isolated from CON^E mice) and of WT *S.Tm* (black circles; $n=3$) or indicated *S.Tm* mutants ($n=3$). Analysis was performed by SYTOX green exclusion and flow cytometry (an example gating for *S.Tm*^{tolC} is shown). The mean value of all experiments is shown (whiskers indicate range). **e**, Cholate sensitivity of individual microbiota strains as analysed in MGAM (2% H₂, 12% CO₂, 86% N₂; Supplementary Table 3; $n=3$, analysis versus growth without inhibitor). Controls, WT *E. coli* ED1a, indicated *S.Tm* strains. Bars indicate median; two-way ANOVA on log-normalized data with Dunnett's multiple comparison test. Dotted lines indicate detection limits. NS, not significant ($P>0.05$); * $P<0.05$, ** $P<0.01$, *** $P<0.005$, **** $P<0.001$.

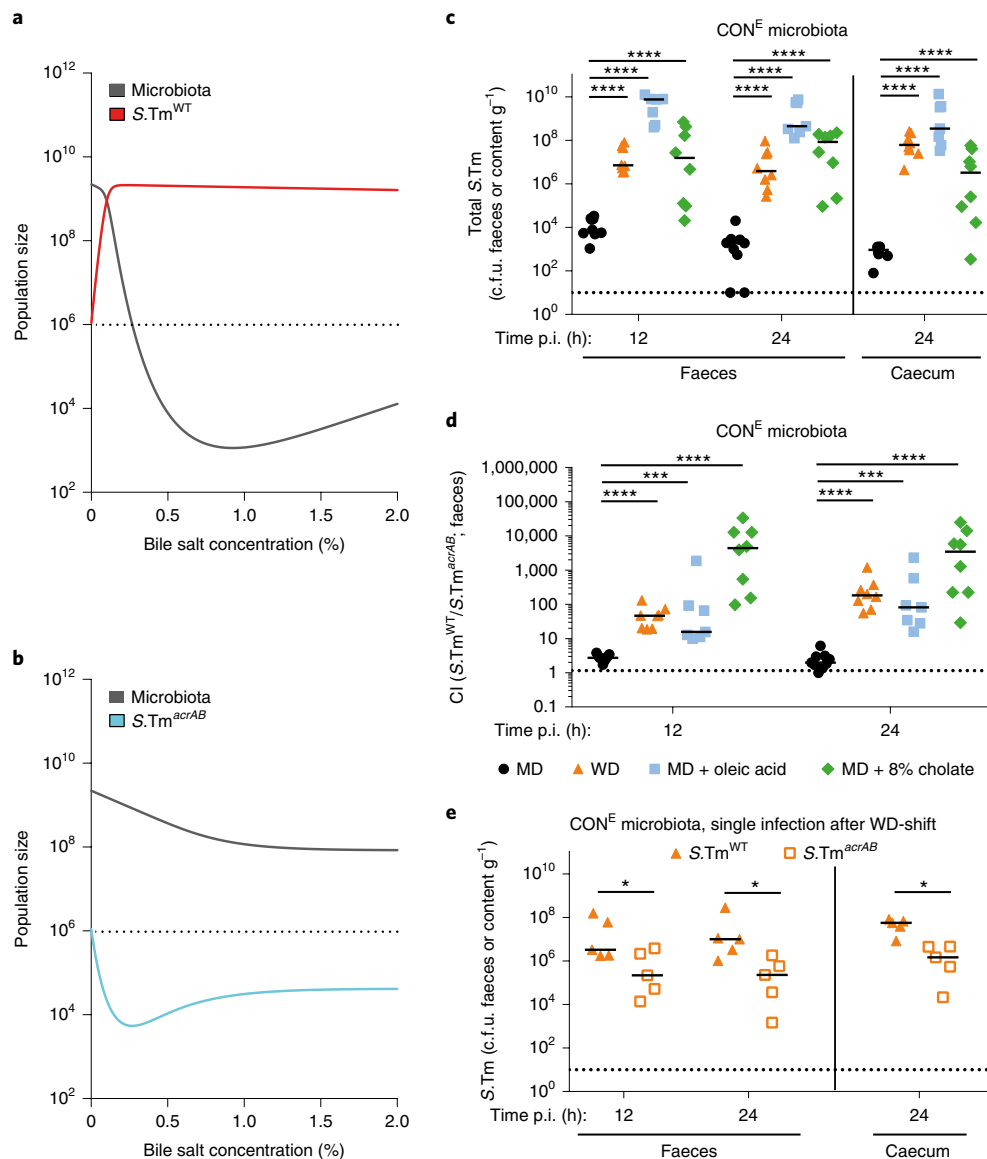


Fig. 3 | Modelling and experimental data validate that bile resistance promotes *S.Tm* growth in the fat-exposed gut. **a, b**, Mathematical model testing if bile-mediated growth inhibition can explain *S.Tm* versus *S.Tm^{acrAB}* blooms after 24 h of growth in the fat-, oleic acid- or cholate-exposed gut (as detailed in the Supplementary Information). **c, d**, Competitive infections. CON^E mice ($n = 7, 8$ and 9) were treated as above and infected with *S.Tm^{WT}* and *S.Tm^{acrAB}* ($1:1; 5 \times 10^7$ c.f.u. total, by gavage). *S.Tm* loads were quantified by plating. In **d**, the competitive index (CI) of *S.Tm^{WT}* versus *S.Tm^{acrAB}* is shown, as analysed by WT isogenic-tagged strain (WITS)-quantitative PCR (qPCR). **e**, Total *S.Tm^{WT}* or *S.Tm^{acrAB}* loads in CON^E mice (C57BL/6, $n = 5$) infected as in Fig. 1a and analysed by plating 24 h p.i. Bars indicate the median; two-way ANOVA on log-normalized data with Dunnett's multiple comparison test. Dotted lines indicate detection limits. * $P < 0.05$, ** $P < 0.01$, *** $P < 0.005$, **** $P < 0.001$.

are well tolerated by *S.Tm* or *E. coli* but not by most Bacteroidetes or Firmicutes strains. Experimental data and modelling indicate that bile salts, which are released during fat digestion, can ablate colonization resistance, that is, when competitive *E. coli* strains are missing. The high prevalence of *E. coli* spp. may explain, why Western-type diets are not associated with human *Salmonella* diarrhoea (Supplementary Discussion). *E. coli* presence and their exact genetic make-up may determine whether colonization resistance is maintained during microbiota disturbance, or not. Future studies should assess the relevant competitive mechanisms (for example, colicins, type 6 secretion systems, oxygen- or iron-depletion^{5,34–38}). Such knowledge might help to identify individuals at risk, and to prevent infections by supplementing potent competitive *E. coli* strains. However, colonization resistance can also be achieved without *E. coli*, as indicated by our experiments in unperturbed CON^E

mice. Nevertheless, when WD-shifts or oleic acid exposure disturb the microbiota, *E. coli* can promote resilience, invigorating colonization resistance after perturbations.

S.Tm growth in the fat-digesting gut relies on AcrAB/TolC efflux pumps^{19,20,39,40}. Most likely, this also holds true for other Enterobacteriaceae like *Citrobacter*, *Escherichia*, *Salmonella*, *Enterobacter*, *Yersinia*, *Klebsiella* and *Shigella* spp. Of note, bile resistance is further modulated by additional factors¹¹; bile can promote pathogen germination⁴² and distant *acrAB*-like genes are also present in other bacteria (Supplementary Fig. 26). Deciphering their contribution to fat/bile-elicited pathogen blooms will be an interesting topic for future work.

Colonization resistance is also compromised by mechanisms other than bile-salt-mediated microbiota perturbation. In cases of fat exposure, pathogen growth on long-chain fatty acids and

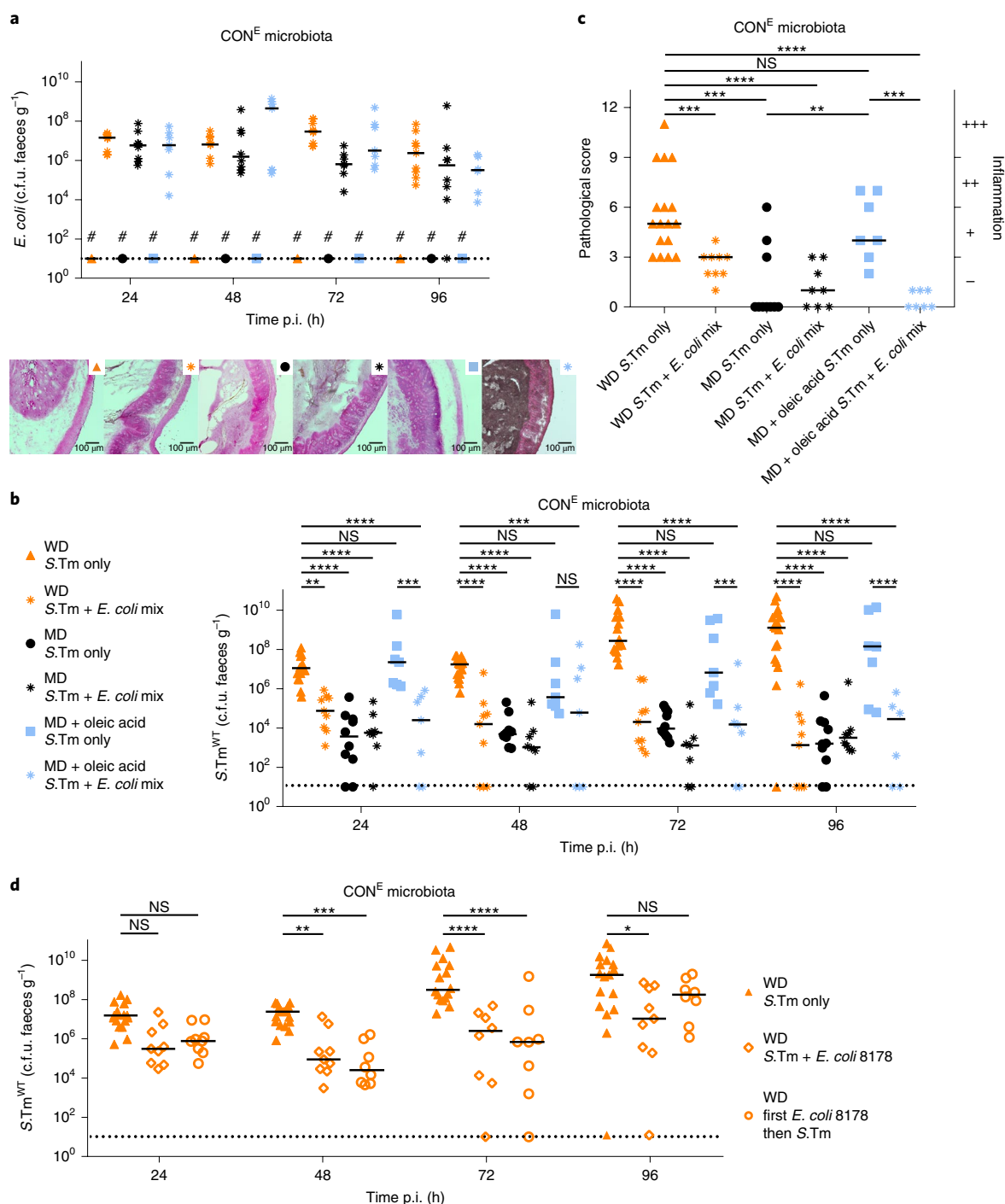


Fig. 4 | *E. coli* limits the *S.Tm* infection after WD-shift or oleic acid gavage. **a–c,** Competitive infection with the *E. coli* mix. CON^E mice ($n=7, 8, 9, 10$ and 17) were treated as in Fig. 1a and infected with WT *S.Tm* and the *E. coli* 8178, CFT073 and Z1324 mix, as indicated (5×10^7 c.f.u. by gavage). *E. coli* and *S.Tm* loads were determined by plating (**a,b**); caecum histopathology 96 h p.i. (**c**). H&E images represent a median sample for a particular treatment. **d**, Competitive infection with *E. coli* 8178. CON^E mice ($n=9$ and 15) were treated as above and gavaged with *E. coli* 8178 and *S.Tm*, as indicated (5×10^7 c.f.u.). Triangles show control mice re-plotted from **b**. Hashtags indicate none detected; bars indicate median values; NS, not significant ($P > 0.05$); * $P < 0.05$, ** $P < 0.01$, *** $P < 0.005$, **** $P < 0.001$, two-way ANOVA on log-normalized data with Dunnett's multiple comparison test (**b,d**) and two-tailed Mann-Whitney U-test (**c**). Dotted lines indicate detection limits.

elicitation of IL-22-induced antimicrobial peptides might contribute in some cases, in particular in the long term. However, in most mice, pathogen growth in the fat-exposed gut begins in the absence of inflammation (Supplementary Fig. 1, step 1b). Fibre deprivation can also promote *C. rodentium*³ and *S.Tm* blooms (Supplementary Fig. 4).

Most probably, additional factors can also alleviate colonization resistance and remain to be identified.

Finally, our findings impinge on the spread of antibiotic resistance plasmids, which is currently of major concern (WHO, 2017)⁴³. As conjugation is contact-dependent and therefore promoted by

high donor and recipient densities¹¹, Enterobacteriaceal blooms elicited by inflammation or antibiotics are known to fuel this process⁶. Our findings suggest that, under certain circumstances, diet shifts may also fuel such bloom-driven plasmid transfer.

We conclude that dietary shifts can be used to study the microbiota–pathogen–host interaction in mice. This may be useful for research on acute infections, protective *E. coli* strains and resistance to plasmid spread.

Methods

Bacterial strains. The *S. enterica* serovar Typhimurium strains used in this study are generally derivatives of the WT strain SL1344 (SB300)⁴⁴. The recipient in PII conjugation experiments was a derivative of *S.Tm* ATCC14028. Deletions in the acetate and propionate metabolism ($\Delta aceA + \Delta prpBCDE$), a key determinant of fatty acid uptake ($\Delta faaL$), and components of the multidrug efflux pump AcrAB-TolC and AcrAD-TolC, were constructed using the lambda Red homologous recombination technique⁴⁵. For selection, the *cat* cassette from pKD3 or the *aphT* cassette from pKD4 were chosen to replace the open reading frames of interest by double homologous recombination. Mutated alleles were subsequently transduced into a fresh strain background by P22 phage transduction. WT isogenic tagged strains (WITS) were provided by A. J. Grant⁴⁶. Tags were transduced into the mutant strains deficient in acetate and propionate metabolism ($\Delta aceA + \Delta prpBCDE$), the long-chain fatty acid import protein ($\Delta faaL$), the multidrug efflux pump AcrAB-TolC and AcrAD-TolC, using P22 phage transduction and subsequent selection on kanamycin or chloramphenicol. Tagged strains were used in competitive infection experiments to test up to six mutant strains against the WT in a given mouse. If indicated, the resistance cassette was removed using pCP20 encoded flippase to generate strains harbouring an in-frame deletion. The replication-incompetent ColE1-like plasmid pAM34 was used to determine the growth rate of *S.Tm* and has been described previously^{47–49}. The plasmid pM972 (*psicA-gfp*) was used to quantify SPI-1 expression in *S.Tm* and has been described previously⁵⁰. The *sicA* promoter (*psicA*) thereby controls the expression of the chromosomal *sicAsipBCDA* operon, which encodes key parts of the SPI-1 type 3 secretion system (T3SS-1). In addition, the mouse commensal *E. coli* 8178 (ref. 6) was used in infection experiments. All constructs were verified by PCR and all strains and their corresponding genotype are listed in Supplementary Table 2.

Ex vivo growth conditions. For infection experiments, bacteria were grown for 12 h at 37 °C shaking (160 rpm) in lysogeny broth (LB) broth and the appropriate antibiotics, sub-cultured for 4 h in LB broth containing 0.3 M NaCl without antibiotics using the same growth conditions and re-suspended in PBS as described previously⁴.

For the minimal inhibitory concentration assays, bacteria were grown overnight at 37 °C shaking (160 rpm) in LB broth containing the appropriate antibiotics. Cultures were adjusted to an OD₆₀₀ of 1 and further diluted 1:2,000 in LB broth to reach 10⁴ c.f.u. per tested condition.

Animals. Male and female 8- to 12-week-old mice were used. The mouse lines used, their microbiota and the presence of *E. coli* are summarized in Supplementary Table 1. All mice were bred under specific (opportunistic and) pathogen-free (SPF, SOPF) conditions in individually ventilated cages in the Rodent Center HCI (RCHCI) or the EPIC mouse facility of ETH. Briefly, the CON^A microbiota harbours a commensal *E. coli* streptomycin-sensitive strain. CON^B mice were re-derived by artificial insemination into a SOPF foster colony and bred in full barrier conditions in individually ventilated cages in the ETH Phenomics Centre (EPIC). 129 Sv/Ev mice (CON^C) were bred in full barrier SOPF conditions in individually ventilated cages in the EPIC facility of ETH (no *E. coli* strains detectable). Oligo-MM¹² (12 strain microbiota; C57BL/6) mice are ex-germ-free mice, which were colonized with a defined consortium of 12 bacterial strains isolated from the murine gut (no *E. coli* strains). These mice are also designated as stable Defined Moderately Diverse Microbiota mice (sDMDMm2), generated in a collaboration between B. Stecher, K. McCoy and A. J. Macpherson (University of Bern)⁵¹. The Oligo mice were bred in open-top cages within flexible film isolators under strict hygienic isolation in a separate room of the EPIC (no *E. coli* strains).

All mice were maintained on the mouse maintenance diet (MD; in the figures, filled black circles; Kliba Nafag, 3537; autoclaved; per weight: 4.5% fat, 18.5% protein, ~50% carbohydrates, 4.5% fibre). As indicated, mice were shifted to a Western-type diet without fibre (WD; filled orange triangles; BioServ, S3282; 60% kcal fat; irradiated; per weight: 36% fat, 20.5% protein, 35.7% carbohydrates, 0% fibre), control diet without fibre (filled black triangles, BioServ, S4031; 16% kcal fat; irradiated; per weight: 7.2% fat, 20.5% protein, 61.6% carbohydrates, 0% fibre), high-fat diet with fibre (filled orange squares, ENVIGO, TD.06414; 60% kcal fat; irradiated; per weight: 34.3% fat, 23.5% protein, 27.3% carbohydrates, 6.6% fibre) or control diet with fibre (filled black squares, ENVIGO, TD.08806; 10.5% kcal fat; irradiated; per weight: 4.2% fat, 18.6% protein, 62.6% carbohydrates, 3.7% fibre) which were fed ad libitum.

Infections and competitive infection experiments. Infections with individual strains, or co-infection experiments with the indicated strain mixtures, were carried out in 8- to 12-week old mice (age- and sex-matched). Mice were kept on MD or switched to WD 24 h before oral infection with 5 × 10⁷ c.f.u. *S.Tm*. Additional experimental groups were treated with PBS or 200, 100, 50 or 10 µl of oleic acid, as indicated (100 µl was used as standard protocol; Sigma-Aldrich) or 4, 6 or 8% cholate (as indicated; cholic acid sodium salt was suspended in PBS and sterile-filtered; 8% was used as standard protocol; EMD Millipore; the dose of 100 µl 8% corresponds to 320 mg per kg body weight) or 12% taurocholate (taurocholic acid sodium salt was suspended in PBS and sterile-filtered; Sigma-Aldrich) 1 h before and 4 h after oral infection with 5 × 10⁷ c.f.u. *S.Tm*. Pretreatment controls with 25 mg streptomycin or ampicillin were performed where indicated, as described previously⁴.

Mouse experiments and data analysis were performed in a non-blinded fashion. To analyse pathogen loads, freshly collected faecal pellets were homogenized in PBS with steel balls in a tissue lyser (Qiagen) and plated on MacConkey agar plates (Oxoid) containing the appropriate antibiotics, as needed (50 µg ml⁻¹ streptomycin, 50 µg ml⁻¹ kanamycin, 15 µg ml⁻¹ chloramphenicol and 20 µg ml⁻¹ ampicillin). The competitive index was calculated by dividing the output ratio (c.f.u. of the mutant/c.f.u. of the WT) by the input ratio (c.f.u. of the mutant/c.f.u. of the WT) of the inoculum. For analysis of bacterial loads in the organs, mice were euthanized by cervical dislocation at the indicated time point (untreated, day 1 p.i., day 4 p.i.), and caecum content, mesenteric lymph nodes, spleen and liver were recovered and homogenized in PBS supplemented with 0.5% tergitol and 0.5% bovine serum albumin. Minimal detectable values were 10 c.f.u. g⁻¹ in faeces and caecum content and 10 c.f.u. per organ in the systemic organs. Each experiment was performed in at least two independent biological replicates including the indicated number of mice and the data were pooled for statistical analysis. Typically, we used at least 5 to 6 mice per group in order to allow analysis by non-parametric statistical tests.

Histological procedures. Pathological scores were determined in a blinded fashion, as described in an earlier study⁴⁶. In brief, samples from liver, spleen, ileum, caecum and colon were embedded in O.C.T. (Sakura), snap-frozen in liquid nitrogen, and stored at -80 °C. Sections (5 µm) were mounted on glass slides, air-dried at room temperature for 2 h, and stained with haematoxylin and eosin (H&E). Pathological score was determined by analysing four markers of inflammation: (1) submucosal oedema, (2) polymorphonuclear granulocyte infiltration into the lamina propria, (3) number of goblet cells harbouring mucus-filled vacuoles and (4) epithelial integrity. Pathological scores range from 0 to 13 arbitrary units (0–3, no or minimal inflammation; 4–6, slight inflammation; 7–9, moderate inflammation; 10–13, profound inflammation).

H&E pictures were taken with an Axioskop 2 plus (Carl Zeiss AG) microscope with a mounted AxioCam HRc (Carl Zeiss AG) camera. AxioVision 4.8 (Carl Zeiss AG) software was used to capture images. Automatic best fit was applied for the best contrast.

WT isogenic tagged strain analysis. Mice were infected with a uniform mixture of the mutant and the WITS of *S.Tm*. A WITS-tag is a unique 40 bp DNA sequence tag within a non-coding region of the chromosome⁴⁶. The faeces and caecum content of infected mice were collected at indicated time points (12 h p.i. and 24 h p.i.) and samples were homogenized in 500 µl PBS (0.5% tergitol and 0.5% bovine serum albumin) using a tissue lyser device (Qiagen; 2 min, 25 Hz). A 250 µl volume of the homogenate was inoculated into 3 ml LB broth culture containing 50 mg ml⁻¹ streptomycin to enrich for the tagged strains for 4 h, then 50 µl of a serial dilution was plated on MacConkey agar (50 mg ml⁻¹ streptomycin) to quantify the density of c.f.u. within each sample. Genomic DNA from enrichment cultures was extracted using the QIAamp DNA Mini Kit (Qiagen). The relative densities of the different WITS were determined by real-time PCR quantification using tag-specific primers⁴⁸. The obtained ratio was multiplied by the number of c.f.u. recovered from selective plating to calculate the absolute loads of each tagged strain.

DNA extraction for 16S rRNA gene sequencing. Caecum content was collected from CON mice kept on the MD, switched to WD or treated with 200 µl of oleic acid and analysed 6, 12 and 24 h after the switch or the treatment. Isolated caecum content samples were immediately shock-frozen in liquid nitrogen and stored at -80 °C. DNA was extracted using the AllPrepDNA/RNA/Protein Kit (Qiagen) with the following changes in the disruption and homogenization steps: 600 ml of RLT buffer and 3 × 4 mm metal beads were added to the tube containing the caecum content and bead-beaten at 10 Hz for 2 min using the Retsch M400. To separate fibres from bacteria, samples were centrifuged at 700g for 2 min at 4 °C. Supernatants containing the bacteria were transferred to a tube containing 0.9 mg of 0.1 mm zirconia beads (OPS Diagnostics) and samples were homogenized at 25 Hz for 5 min. Before the transfer of the lysates to the QIAshredder column (Qiagen), lysates were pre-heated to 25 °C. The QIAshredder columns were centrifuged at 13,000g for 3 min at room temperature for further homogenization. The flowthrough was centrifuged for 3 min at full speed to pellet the cell debris. The supernatants were loaded on the DNA columns and DNA was extracted

according to the manufacturer's instructions with the modification that DNA was eluted in 100 µl EB.

Library preparation and 16S rRNA gene sequencing. The library was produced using the NEXTFlex 16S V4 Amplicon-Seq Kit 2.0 (barcodes 1–96; Bioo Scientific). The input concentration of genomic DNA was adjusted to 30 ng µl⁻¹ for each PCR reaction. The library preparation was performed following the manufacturer's instructions with the differences that the reaction volume was reduced to 25 µl per reaction and a modified primer pair was used for the first PCR reaction. Instead of the primer pair 515f-806r that is supplied with the kit, the degenerate primers 515F (5'-GTGYCAGCMGCCGCGGTAA-3') and 806rB (5'-GGACTACNVGGGTWTCTAAT-3'), as described in refs. ^{52,53}, were applied. The first PCR reaction was performed using Q5 High-Fidelity DNA polymerase (BioConcept (NEB)) under the following cycle conditions: (1) initial denaturation, 95 °C for 4 min; (2) denaturation, 95 °C for 30 s; (3) annealing, 56 °C for 30 s; (4) extension, 72 °C for 90 s; (5) final extension, 72 °C for 4 min. Cycles 2 to 4 were repeated eight times. After each PCR reaction, the PCR products were cleaned from oligos and nucleotides by AMPure XP magnetic beads (Beckman Coulter). The cleaned PCR product was eluted in 20 µl of resuspension buffer and used in a second PCR reaction with barcoded primers or for producing multiplexed samples. The quantity of amplicons was measured using a Qubit fluorometer. The quality of the amplicons was verified using a fragment analyzer (Advanced Analytical). The length of the amplicons after barcoding was ~450 bp. PCR products were adjusted to a final concentration of 60 ng DNA per 20 µl of multiplexed sample. Paired end read sequencing was performed on the Illumina MiSeq platform at the Functional Genomics Center, Zürich.

Analysis of microbiota composition. For CON^E mice, raw sequencing data were processed using custom scripts to execute several commands of the USEARCH software (version 9.1.13): paired reads were merged and quality-filtered using the fastq_mergepairs command with default settings. Merged reads were filtered using the fastq_filter command (-fastq_maxee 0.1) and only merged reads with perfect primer matches and a minimum length of 100 bp were selected. Sequences were de-replicated using the fastq_uniques command and clustered into operational taxonomic units (OTUs) at 97% using the cluster_otus command (-minsize 2), which also removed chimeric sequences. OTU abundances for each sample were quantified using the usearch_global command (-strand both; -id 0.97). Taxonomic annotation was performed by querying OTU sequences against the SILVA database (version 128) using the usearch_global command (-id 0.90; -maxaccepts 20; -maxrejects 500; -strand both; -top_hits_only). For Oligo mice, strain-specific qPCR measurements were transformed into relative abundances.

Further analyses were performed in RStudio (version 1.0.143 based on R version 3.3.3) using the libraries vegan and ggplot2. Read counts were rarefied to 20,000 reads per sample. For performing a principal component analysis, Euclidean distances after Hellinger transformation were computed between samples using the vegdist function.

Determination of *S.Tm* growth rates in the gut. *S.Tm* growth rates in the gut were assessed using replication-incompetent plasmid pAM34, which has been described previously^{48,49}. Briefly, pAM34 is a ColE1-like vector in which the replication of the plasmid is under the control of the LacI repressor, whereby plasmid replication only occurs in the presence of isopropyl β-D-1-thiogalactopyranoside (IPTG)⁴⁷. *S.Tm* carrying the pAM34 plasmid was therefore cultured for 12 h in the presence of 1 mM IPTG in LB broth and in the absence of antibiotics. Cultures were diluted 1:20 into fresh LB broth without IPTG and sub-cultured for 3 h at 37 °C. Inocula for in vivo infections were prepared as described previously⁴. Oligo mice were kept on the MD, switched to WD 24 h before infection or treated with 100 µl oleic acid 1 h before and 4 h after the infection with 5 × 10⁷ c.f.u. *S.Tm* carrying pAM34. Concurrently, the inoculum was serially diluted into fresh LB broth without IPTG and cultured overnight at 37 °C to generate a standard curve relating plasmid loss to generations undergone for each experiment. pAM34-carrying bacteria within the overnight cultures and the faeces were determined by selective plating on agar plates containing 100 µg ml⁻¹ ampicillin and 1 mM IPTG. To quantify the total population size, samples were further plated on agar plates containing 50 µg ml⁻¹ streptomycin. The fraction of pAM34-carrying bacteria was calculated using the ratio of pAM34-carrying c.f.u. to the total population c.f.u. and generations estimated by interpolation from the matched standard curve.

Real-time qPCR for analysis of transcript levels. The caecum mid-segments were rinsed in cold sterile PBS and the washed tissue was shock-frozen in RNAlater (Qiagen) using liquid nitrogen and stored at -80 °C until RNA extraction. Total RNA was extracted using the RNeasy Mini Kit (Qiagen). The RNA concentration of each sample was adjusted to 0.125 µg µl⁻¹ and samples were reverse-transcribed using the RT2 HT First Strand cDNA kit (Qiagen). Custom RT2 Profiler PCR arrays and primer assays (Qiagen) were run with Universal FastStart SYBR Green Master (ROX; Roche) on the StepOne Plus real-time PCR system (Applied Biosystems) using the following cycling conditions: (1) initial denaturation, 95 °C for 14 min; (2) denaturation, 94 °C for 15 s; (3) annealing, 61 °C for 30 s; (4) extension, 72 °C for 20 s. Cycles 2–4 were repeated 40 times. Relative transcript

levels were normalized to actin-b. The upper limit of C_q was fixed to 38 cycles. All procedures were performed according to the manufacturer's instructions.

Total gastrointestinal transit time. Total gastrointestinal (GI) transit time was assessed using the carmine red dye assay, which has been described previously⁵⁴. Briefly, carmine red (Sigma-Aldrich) was prepared as a 6% (w/v) solution in 0.5% methylcellulose (Sigma-Aldrich) and autoclaved before use. CON mice were kept on the MD, switched to WD 24 h before the assay or treated with 100 µl oleic acid 1 h before and 4 h after the application of 150 µl carmine red dye. CON mice treated twice with 0.9% saline served as a control for the loperamide treatment. Animals were not fasted beforehand. Faeces were collected every 30 min (up to 9 h from time of gavage) and evaluated for the presence of the carmine red dye. The time from gavage to initial appearance of carmine red in the faeces was recorded as the total GI transit time for the respective animal.

Mass spectrometry. Duodenum and caecum content of mice kept on the MD, switched to WD or treated with two doses of 100 µl oleic acid as described previously were collected at 6, 9, 12 or 24 h after the switch to WD or treatment with oleic acid. Different gut contents were normalized by weight and suspended in 15 times more (w/v) ultrapure water using device tissue lyser (Qiagen; 3 min 25 Hz). Suspended samples were centrifuged (5 min, full speed) and 70 µl of the supernatant was shock-frozen in liquid nitrogen and stored at -80 °C. For mass spectrometric analysis, samples were thawed and centrifuged at 20,000g for 10 min at 4 °C. Supernatant was transferred to 96-well storage plates and measured in different dilutions. Relative metabolites levels were quantified with an Agilent 6550 Q-TOF mass spectrometer (Agilent Technologies) by non-targeted flow injection analysis as described previously⁵⁵. Profile spectra with high mass accuracy were recorded from 50 to 1,000 *m/z* in negative ionization mode. The common mass axis after sample alignment was recalibrated using known frequently occurring metabolite ions. Ions were finally annotated based on accurate mass comparison using 1 mDa mass tolerance against a list of compounds derived from the KEGG database⁵⁶ assuming single charged ions after deprotonation.

To quantify cholate we employed ultra-performance liquid chromatography-high-resolution heated electrospray ionization mass spectrometry (UPLC HR HESI-MS). The data were recorded on a Thermo Scientific Q Exactive Hybrid Quadrupole-Orbitrap mass spectrometer coupled to a Dionex Ultimate 3000 UPLC. According to ref. ⁵⁷ we used a solvent gradient (A = H₂O, 0.1% formic acid, B = acetonitrile, 0.1% formic acid with B at 5% from 0 to 0.5 min, 5–20% from 0.5 to 1 min, 20–25% from 1 to 2 min, 25% from 2 to 5.5 min, 25–30% from 5.5 to 6 min, 30% from 6 to 8 min, 30–35% from 8 to 9 min, 35–75% from 9 to 17 min, 75–100% from 17 to 18 min and 100% from 18 to 19 min at a flow rate of 0.5 ml min⁻¹) on a Phenomenex Kinetex 2.6 µm XB-C18 100 Å (150 × 4.6 mm) column at 45 °C. The mass spectrometer was operated in negative ionization mode at a scan range of 200–800 *m/z* and a resolution of 75,000. The spray voltage was set to 3.0 kV, the S-lens to 1, the auxiliary gas heater temperature to 438 °C and the capillary temperature to 270 °C. Further parameters used were AGC target (1e6), maximum injection time (200 ms), microscans (1), sheath gas (53), aux gas (14) and sweep gas (3). Absolute quantification was achieved by using cholate from Sigma-Aldrich as a standard. The standard curve was recorded with water-diluted concentrations of 10 ng ml⁻¹, 50 ng ml⁻¹, 100 ng ml⁻¹, 250 ng ml⁻¹, 500 ng ml⁻¹, 1 µg ml⁻¹, 10 µg ml⁻¹ and 50 µg ml⁻¹ from a 1 mg ml⁻¹ cholate stock solution. Data obtained from undiluted sample supernatants were analysed for cholate retention time and ion adduct [M-H + HCO₂H]⁻ = 453.2857 *m/z* with a mass tolerance of 5 ppm. Concentrations were calculated using the Thermo Xcalibur 2.2 Quan browser.

Flow cytometric analysis of immune cells of the caecal mucosa. Mice were euthanized and the caecum was excised and cut open longitudinally. To dislodge epithelial cells, the caecum tissue was cut into small pieces and incubated twice in 14 ml PBS (5 mM EDTA, 15 mM HEPES, 10% FCS; 20 min, 37 °C, mildly shaking). Subsequently, samples were washed in RPMI (30% FCS) and transferred to RPMI (1 mg ml⁻¹ collagenase VIII (Sigma), 0.2 mg ml⁻¹ DNase I (Roche)). The tissue pieces were digested by mildly shaking for 1 h at 37 °C. The digested tissue was passed through a 70 µm cell strainer and washed with RPMI. The cells were resuspended in RPMI and carefully pipetted onto a Nycoprep (Progen) 1.077 matrix. After centrifugation (30 min, 400g), cells from the interphase were collected, rinsed with RPMI (15% FCS) and suspended in PBS (1% FCS). For intracellular staining, we first performed surface marker staining. Then, cells were fixed and permeabilized for 40 min at room temperature in the dark with Foxp3 Fix/Perm buffer (eBioscience/Thermo Fisher). Subsequently, cells were washed with permeabilization/wash buffer (eBioscience/Thermo Fisher) and stained for 40 min at room temperature in the dark. Antibodies/dyes used in this study: CD45 (30-F11, Biologend), CD4 (RM4-5, Thermo Fischer), Foxp3 (FJK-16s, Thermo Fischer), F4/80 (BM8, Biologend), CD103 (2E7, Biologend), MHCII (M5/114.15.2, Biologend), CD11b (M1/70, Biologend), CD11c (N418, Biologend), SYTOX blue (Invitrogen) and Zombie-NIR (Biologend).

Flow cytometric analysis of SPI-1 expression using the plasmid pM972. Overnight cultures of *S.Tm* carrying the plasmid pM972 were set up in LB

broth containing 50 mg ml⁻¹ ampicillin, and inocula were prepared as previously described⁴. CON mice were pretreated with ampicillin 24 h before infection, switched to WD 24 h before infection or treated with 100 µl oleic acid 1 h before and 4 h after infection with 5 × 10⁷ c.f.u. S.Tm carrying pM972. Faecal samples were collected 12, 18 and 24 h p.i. and the caecum content was collected 24 h p.i. after elimination of the mice. All collected samples were diluted 1:20 (w/v) in sterile PBS. A 1 µl sample of caecum content was stained in 50 µl of PBS containing anti-O5 rabbit polyclonal antiserum (1:200 vol/vol) and incubated for 10 min. PBS (200 µl) was added to wash the cells. The samples were then centrifuged (4,000 r.p.m., 20 min) and supernatant was removed. Bacterial cells were suspended in 200 µl PBS. Samples were measured using an LSRII flow cytometer (Becton Dickinson) with both forward- and side-scatter parameters at a low, non-zero threshold value and acquired on a logarithmic scale. Data were processed using the Flowjo software (Treestar).

Flow cytometric assay for measuring cholate-dependent killing. S.Tm WT strain and the mutant strains $\Delta tolC$ and $\Delta acrB$ were grown overnight at 37 °C while shaking (160 r.p.m.) in LB broth containing the appropriate antibiotics. Ileum, caecum and colon content of untreated CON mice was collected and diluted 1:20 (w/v) in sterile M9 base salts. Different concentrations (0.125, 0.5, 1, 2 and 8%) of cholate were dissolved in M9 base salts. M9 base salts alone served as a control for potential killing of the gut microbiota on contact with oxygen. A 100 µl volume of M9 base salts only or the respective cholate solutions was pipetted into a 96-well plate, mixed with 1 µl of the different gut contents (harbouring microbiota) or the three S.Tm strains and incubated for 20 min at room temperature. Afterwards, samples were centrifuged (4,000 r.p.m., 20 min), supernatant was removed and bacterial cells were suspended in 200 µl PBS containing SYTOX green (1:5,000 vol/vol; Invitrogen, ThermoFisher) to detect bacteria with loss of membrane integrity. This dye can only penetrate and stain the DNA of microorganisms when the cell membrane is compromised. The SYTOX-positive (SYTOX⁺) fraction was quantified using a LSRII flow cytometer (Becton Dickinson) with both forward- and side-scatter parameters at a low, non-zero threshold value and acquired on a logarithmic scale. Data were processed using the Flowjo software (Treestar).

Minimal inhibitory concentration assay. The sensitivity of S.Tm WT, the mutants deficient in the AcrAB-TolC and AcrAD-TolC efflux pump against certain antimicrobials and primary bile salts, was assessed using the minimal inhibitory concentration (MIC) assay, which has been described previously⁵⁸. Briefly, overnight cultures of the different strains were adjusted to an optical density at 600 nm (OD₆₀₀) of 1 and further diluted 1:2,000 in LB broth to obtain 1 × 10⁴ c.f.u. per well (assay was performed in sterile 96-well plates). Stock solutions of the different antimicrobial agents were generated in LB broth as the following: 0.0625 µg ml⁻¹ ciprofloxacin, 100 µg ml⁻¹ rifampicin, 100 µg ml⁻¹ erythromycin, 6.25 µg ml⁻¹ tetracycline, 10 µg ml⁻¹ polymyxin B, 8% cholate and 8% taurocholate. Each stock was further serially diluted 1:2 and 50 µl each of the different antimicrobial agent solutions was mixed with 50 µl of the respective inocula. The plates were incubated at 37 °C and growth was measured at 0, 4, 6, 8 and 24 h by measuring the OD₆₀₀ with a Spectramax plus system (Bucher Biotec). During the incubation between 8 and 24 h of growth, plates were sealed with Breathe-easier tape (Sigma-Aldrich) and covered with the lid of the 96-well plates. The function $y = A + Ce^{-\frac{B(x-M)}{C}}$ was fit to the OD₆₀₀ values dependent on the log₁₀ of the drug concentration⁵⁹. The MIC was then calculated as the drug concentration where the line $y = A$ (the lower asymptote of y) intersects with the line tangential at $x = M$. The 50% MIC was calculated as the drug concentration where the same line tangential intersects with the line $y = 0.5 \times (C - A)$, the y value where growth is half-maximal. The 95% and 5% confidence intervals were calculated by adding and subtracting the standard error of the fit multiplied by the 95% entry of the Student t statistic for 32 degrees of freedom to and from the value of the fit at $y = 0.5 \times (C - A)$, respectively.

Determination of cholate sensitivity across individual microbiota strains.

Experiments were performed under anoxic conditions (2% H₂, 12% CO₂ in N₂) in an anaerobic chamber (Coy Laboratory Products) using pre-reduced modified Gifu anaerobic medium (MGAM, HyServe) at 37 °C. Strains were grown twice overnight before recording growth curves. Bacterial growth in the presence of the indicated concentrations of sodium cholate or taurocholate (Sigma Aldrich) was monitored in NUNC 96-well U-bottomed plates (Fisher Scientific) using a starting OD at 578 nm of 0.01 for all strains. Plates were sealed with breathable membranes (Breathe-Easy) and incubated at 37 °C without shaking. The OD₅₇₈ was measured every hour for 24 h after 30 s of linear shaking with a microplate spectrophotometer (EON, Biotek) by a microplate stacker (Biostack 4, Biotek). Time points with sudden spikes in OD (for example, caused by condensation) were removed. All plates contained medium-only control wells to allow comparison to unperturbed growth. For each strain, control growth curves were used to determine the time of transition from exponential to stationary phase, and all growth curves were truncated using this time point. To quantify growth, we calculated the area under the curve (AUC) using the trapezoidal rule. For baseline correction, we assumed a constant shift and subtracted the same shift from all time points of the growth curves such that the starting OD was zero. AUCs were normalized by dividing the AUC for specific cholate concentrations by the mean AUC of unperturbed growth

of the same strain within the same plate. Mean normalized AUCs from three biological replicates are shown.

Mathematical modelling. To understand how the sensitivities of S.Tm and the microbiota to an increase in bile concentration will change the ability of S.Tm to establish a transiently stable population in the mouse intestine, we devised a simple mathematical model. In the following, we will introduce the different parameters of the model and explain how they were derived from our own measurements or from published data (see also Supplementary Table 6 for a list of all parameters).

Dependence of bacterial growth on bile salt concentrations. We used the data describing the effect of different cholate concentrations on the growth of the different microorganisms (Fig. 2e and Supplementary Fig. 13) to infer a mathematical relationship between bile concentration and bacterial growth, both for S.Tm and the murine microbiota. To do this, we performed linear regression on the natural logarithm of the normalized AUC values, in a concentration range between 0 and 1% cholate (Supplementary Fig. 13), separately for the bacterial species tested. The slope of these regression lines is the rate parameter for the exponential decay of growth rate with bile salt concentration. Importantly, this way to estimate the dependence of growth on cholate is independent of the differences in growth yields and lag times between strains. Owing to the nature of the above AUC measurement, this estimation of growth assumes that all strains start growing exponentially after the lag time of the 0% sample of a given strain (which is reasonable given our data), and the measurement stops at the time when the 0% sample reaches saturation. The rate of growth between these two time points is then described by a single exponential function, effectively averaging over potential growth transitions that happen during this time (Supplementary Fig. 14).

To obtain a value for the overall growth dependence of the microbiota (as opposed to the single microbiota members) on cholate concentration, we simply took the unweighted average of the slope of all members of the murine microbiota. Note that this is a crude way of assuming the true value, as taking the unweighted average assumes equal numbers of all bacteria in the microbiota, which is an oversimplification.

With this, we have parameters for the rate of decrease in growth rate with bile salt concentration, for both S.Tm and the murine microbiota (w/o *E. coli*). We denote these rates as k_S and k_M , respectively. We can now formulate expressions for the growth rates of S.Tm and the microbiota, r_S and r_M , depending on the bile salt concentration:

$$r_S = r_{S,\max} \times e^{-k_S \times BA}$$

$$r_M = r_{M,\max} \times e^{-k_M \times BA}$$

where $r_{S,\max}$ and $r_{M,\max}$ are the maximum growth rates of S.Tm and the microbiota (that is, the growth rates at $BA = 0$), respectively. Maximum growth rates were set to 1.1 h⁻¹ for both the microbiota and S.Tm. This is based on measured data for both S.Tm (measured growth rate is 1.10 h⁻¹) and *Bacteroides thetaiotaomicron* (measured growth rate 1.05 h⁻¹ (ref. 60)).

Estimation of initial population sizes. To estimate the initial S.Tm^{WT} and S.Tm^{acrAB} (mutant with non-functional AcrAB/TolC efflux pump) population size S , we used the experimental inoculum size used for the infections, $S = 5 \times 10^7$. The microbiota population size without bile salt was set to be 1×10^{11} cells⁶¹, and the results shown in Fig. 3a,b were generated using $M = 10^{11}$ consistently.

It is of interest that this number reflects a steady state of microbiota growth and loss through outflow. Inhibition of growth by bile salt, assuming outflow to be unchanged, could therefore lead to a decrease in microbiota population size that is directly proportional to microbiota growth, and can thus be modelled using the same kinetics (see previous paragraph for the estimation of parameters):

$$M(BA) = 10^{11} \times e^{-k_M \times BA}$$

We tested how adding this dependence of the initial microbiota population size on bile concentrations to the model changes the outcome, and show the results below (see Methods, 'Model results').

Population dynamics. To describe the population dynamics of S.Tm and the microbiota, we now formulate the following differential equations, where S denotes S.Tm population size and M the microbiota population size:

$$\frac{dS}{dt} = S \times (r_S - (S + M) \times d)$$

$$\frac{dM}{dt} = M \times (r_M - (S + M) \times d)$$

where d is a description of clearance and death, introducing an effective carrying capacity for the total population size of $(S + M)$, which dynamically relates the two populations.

Model results. The results for the modelled competition of *S.Tm^{WT}* and *S.Tm^{acrAB}* strains against the murine microbiota after 24 h with constant initial microbiota population sizes are depicted in Fig. 3a,b.

In Supplementary Fig. 15, we show in addition how changing the initial microbiota population size in response to bile (see Methods, 'Estimation of initial population sizes') affects the results of this competition. This modification of the model leads to increasingly smaller *M* with increasing bile salt concentrations. In the case of competition of *S.Tm^{WT}* against the microbiota, this only leads to small quantitative differences in realistic bile salt concentrations (that is, below 1%, Supplementary Fig. 15a) when compared to the model with constant initial microbiota population size (Fig. 3a,b). However, in the case of competition of the *S.Tm^{acrAB}* strain against the microbiota (Supplementary Fig. 15b), we observe a qualitative difference in the observed curves when comparing to the model with constant initial microbiota population size: at high bile salt concentrations, the *S.Tm^{acrAB}* population increases (Supplementary Fig. 15b, cyan line). There is a simple explanation for this: very little growth happens in either population at these bile salt concentrations, and the observed population sizes are therefore largely determined by the initial population size, and, because the initial microbiota population size becomes smaller with increasing bile salt concentration, but the initial *S.Tm^{acrAB}* population size remains constant, we observe the behaviour shown in Supplementary Fig. 15b.

Numerical simulations. To solve the system numerically, we used the function 'ode' in the package deSolve⁶² in the R language of statistical computing⁶³. The time resolution of the simulations was 12 min.

Sequence analysis of *arcAB*- and *tolC*-like genes. The *Salmonella* protein sequences were queried against the full proteome sequences of the other 27 tested strains by BLASTp. Targets with an alignment bitscore of at least 60 were considered as homologues of *acrAB/tolC*. Phylogenetic relationship, cholerae resistance (data represent average AUC values from Fig. 2e) and bitscores were visualized using iTOL v3⁶⁴.

Statistical analysis. Sample size was determined from the data of previous studies. Scientists were not blinded for the assignment of the experiments and the data analysis. The exact Mann–Whitney U-test was performed when two groups were compared. One-way ANOVA was carried out when two or more treatment groups were compared. When time courses/different sampling sides were compared with two or more groups, two-way ANOVA was used to determine significance. Statistical analysis was performed by the software Graphpad Prism Version 7.02 for Windows (GraphPad Software). *P* values of less than 0.05 were considered to indicate statistical significance.

Ethical statement. All animal experiments were reviewed and approved by the Kantonales Veterinäramt, Zürich (licence 222/2013 + 193/2016) and are subject to the Swiss animal protection law (TschG).

Reporting Summary. Further information on research design is available in the Nature Research Reporting Summary linked to this article.

Data availability

16S rRNA raw reads have been deposited at the European Nucleotide Archive (ENA) with accession no. PRJEB33890. All other data needed to evaluate the conclusions in this Article are presented in the paper or the Supplementary Information. Any additional data can be requested from the corresponding author.

Received: 22 August 2018; Accepted: 23 August 2019;

Published online: 7 October 2019

References

- Stecher, B., Berry, D. & Loy, A. Colonization resistance and microbial ecophysiology: using gnotobiotic mouse models and single-cell technology to explore the intestinal jungle. *FEMS Microbiol. Rev.* **37**, 793–829 (2013).
- David, L. A. et al. Diet rapidly and reproducibly alters the human gut microbiome. *Nature* **505**, 559–563 (2014).
- Desai, M. S. et al. A dietary fiber-deprived gut microbiota degrades the colonic mucus barrier and enhances pathogen susceptibility. *Cell* **167**, 1339–1353 (2016).
- Barthel, M. et al. Pretreatment of mice with streptomycin provides a *Salmonella enterica* serovar Typhimurium colitis model that allows analysis of both pathogen and host. *Infect. Immun.* **71**, 2839–2858 (2003).
- Brugiroux, S. et al. Genome-guided design of a defined mouse microbiota that confers colonization resistance against *Salmonella enterica* serovar Typhimurium. *Nat. Microbiol.* **2**, 16215 (2016).
- Stecher, B. et al. Gut inflammation can boost horizontal gene transfer between pathogenic and commensal Enterobacteriaceae. *Proc. Natl Acad. Sci. USA* **109**, 1269–1274 (2012).
- Arkan, M. C. et al. IKK- β links inflammation to obesity-induced insulin resistance. *Nat. Med.* **11**, 191–198 (2005).
- Kim, K. A., Gu, W., Lee, I. A., Joh, E. H. & Kim, D. H. High fat diet-induced gut microbiota exacerbates inflammation and obesity in mice via the TLR4 signaling pathway. *PLoS ONE* **7**, e47713 (2012).
- Moya-Perez, A., Neef, A. & Sanz, Y. *Bifidobacterium pseudocatenulatum* CECT 7765 reduces obesity-associated inflammation by restoring the lymphocyte-macrophage balance and gut microbiota structure in high-fat diet-fed mice. *PLoS ONE* **10**, e0126976 (2015).
- Hwang, D. H., Kim, J. A. & Lee, J. Y. Mechanisms for the activation of Toll-like receptor 2/4 by saturated fatty acids and inhibition by docosahexaenoic acid. *Eur. J. Pharm.* **785**, 24–35 (2016).
- Stecher, B., Maier, L. & Hardt, W. D. 'Blooming' in the gut: how dysbiosis might contribute to pathogen evolution. *Nat. Rev. Microbiol.* **11**, 277–284 (2013).
- Reddy, B. S., Mangat, S., Sheinfil, A., Weisburger, J. H. & Wynder, E. L. Effect of type and amount of dietary fat and 1,2-dimethylhydrazine on biliary bile acids, fecal bile acids and neutral sterols in rats. *Cancer Res.* **37**, 2132–2137 (1977).
- Reddy, B. S. Diet and excretion of bile acids. *Cancer Res.* **41**, 3766–3768 (1981).
- Cummings, J. H. et al. Influence of diets high and low in animal fat on bowel habit, gastrointestinal transit time, fecal microflora, bile acid and fat excretion. *J. Clin. Invest.* **61**, 953–963 (1978).
- Begley, M., Gahan, C. G. & Hill, C. The interaction between bacteria and bile. *FEMS Microbiol. Rev.* **29**, 625–651 (2005).
- Islam, K. B. et al. Bile acid is a host factor that regulates the composition of the cecal microbiota in rats. *Gastroenterology* **141**, 1773–1781 (2011).
- Urdaneta, V. & Casadesu, J. Interactions between bacteria and bile salts in the gastrointestinal and hepatobiliary tracts. *Front. Med.* **4**, 163 (2017).
- MacConkey, A. T. Bile salt media and their advantages in some bacteriological examinations. *J. Hyg.* **8**, 322–334 (1908).
- Buckley, A. M. et al. The AcrAB-TolC efflux system of *Salmonella enterica* serovar Typhimurium plays a role in pathogenesis. *Cell. Microbiol.* **8**, 847–856 (2006).
- Nishino, K., Latifi, T. & Groisman, E. A. Virulence and drug resistance roles of multidrug efflux systems of *Salmonella enterica* serovar Typhimurium. *Mol. Microbiol.* **59**, 126–141 (2006).
- Devkota, S. et al. Dietary-fat-induced taurocholic acid promotes pathobiont expansion and colitis in *Il10^{-/-}* mice. *Nature* **487**, 104–108 (2012).
- Stecher, B. et al. *Salmonella enterica* serovar Typhimurium exploits inflammation to compete with the intestinal microbiota. *PLoS Biol.* **5**, 2177–2189 (2007).
- Winter, S. E. et al. Gut inflammation provides a respiratory electron acceptor for *Salmonella*. *Nature* **467**, 426–429 (2010).
- Winter, S. E. et al. Host-derived nitrate boosts growth of *E. coli* in the inflamed gut. *Science* **339**, 708–711 (2013).
- Raffatelli, M. et al. Lipocalin-2 resistance confers an advantage to *Salmonella enterica* serotype Typhimurium for growth and survival in the inflamed intestine. *Cell Host Microbe* **5**, 476–486 (2009).
- Litvak, Y., Byndloss, M. X. & Baumler, A. J. Colonocyte metabolism shapes the gut microbiota. *Science* **362**, eaat9076 (2018).
- Miki, T., Goto, R., Fujimoto, M., Okada, N. & Hardt, W. D. The bactericidal lectin RegIII β prolongs gut colonization and enteropathy in the streptomycin mouse model for *Salmonella* diarrhea. *Cell Host Microbe* **21**, 195–207 (2017).
- Miki, T., Holst, O. & Hardt, W. D. The bactericidal activity of the C-type lectin RegIII β against Gram-negative bacteria involves binding to lipid A. *J. Biol. Chem.* **287**, 34844–34855 (2012).
- Mukherjee, S. et al. Antibacterial membrane attack by a pore-forming intestinal C-type lectin. *Nature* **505**, 103–107 (2014).
- Lopez, C. A. et al. Phage-mediated acquisition of a type III secreted effector protein boosts growth of *Salmonella* by nitrate respiration. *mBio* **3**, e00143-12 (2012).
- Berg, R. D. The indigenous gastrointestinal microflora. *Trends Microbiol.* **4**, 430–435 (1996).
- Piddock, L. J. Multidrug-resistance efflux pumps—not just for resistance. *Nat. Rev. Microbiol.* **4**, 629–636 (2006).
- Wotzka, S. Y. et al. Microbiota stability in healthy individuals after single-dose lactulose challenge—a randomized controlled study. *PLoS ONE* **13**, e0206214 (2018).
- Litvak, Y. et al. Commensal Enterobacteriaceae protect against *Salmonella* colonization through oxygen competition. *Cell Host Microbe* **25**, 128–139 (2019).
- Sana, T. G. et al. *Salmonella* Typhimurium utilizes a T6SS-mediated antibacterial weapon to establish in the host gut. *Proc. Natl Acad. Sci. USA* **113**, E5044–E5051 (2016).
- Deriu, E. et al. Probiotic bacteria reduce *Salmonella* Typhimurium intestinal colonization by competing for iron. *Cell Host Microbe* **14**, 26–37 (2013).
- Nedialkova, L. P. et al. Temperate phages promote colicin-dependent fitness of *Salmonella enterica* serovar Typhimurium. *Environ. Microbiol.* **18**, 1591–1603 (2016).
- Conway, T. & Cohen, P. S. Commensal and pathogenic *Escherichia coli* metabolism in the gut. *Microbiol. Spectr.* **3**, MBP-0006-2014 (2015).

39. Baucheron, S. et al. AcrAB-TolC directs efflux-mediated multidrug resistance in *Salmonella enterica* serovar Typhimurium DT104. *Antimicrob. Agents Chemother.* **48**, 3729–3735 (2004).
40. Eaves, D. J., Ricci, V. & Piddock, L. J. Expression of *acrB*, *acrF*, *acrD*, *marA* and *soxS* in *Salmonella enterica* serovar Typhimurium: role in multiple antibiotic resistance. *Antimicrob. Agents Chemother.* **48**, 1145–1150 (2004).
41. Urdaneta, V. & Casadesus, J. Adaptation of *Salmonella enterica* to bile: essential role of AcrAB-mediated efflux. *Environ. Microbiol.* **20**, 1405–1418 (2018).
42. Theriot, C. M. et al. Antibiotic-induced shifts in the mouse gut microbiome and metabolome increase susceptibility to *Clostridium difficile* infection. *Nat. Commun.* **5**, 3114 (2014).
43. Rozwandowicz, M. et al. Plasmids carrying antimicrobial resistance genes in Enterobacteriaceae. *J. Antimicrob. Chemother.* **73**, 1121–1137 (2018).
44. Hoiseh, S. K. & Stocker, B. A. Aromatic-dependent *Salmonella* Typhimurium are non-virulent and effective as live vaccines. *Nature* **291**, 238–239 (1981).
45. Datsenko, K. A. & Wanner, B. L. One-step inactivation of chromosomal genes in *Escherichia coli* K-12 using PCR products. *Proc. Natl Acad. Sci. USA* **97**, 6640–6645 (2000).
46. Grant, A. J. et al. Modelling within-host spatiotemporal dynamics of invasive bacterial disease. *PLoS Biol.* **6**, e74 (2008).
47. Gil, D. & Bouche, J. P. ColE1-type vectors with fully repressible replication. *Gene* **105**, 17–22 (1991).
48. Kaiser, P. et al. Cecum lymph node dendritic cells harbor slow-growing bacteria phenotypically tolerant to antibiotic treatment. *PLoS Biol.* **12**, e1001793 (2014).
49. Moor, K. et al. High-avidity IgA protects the intestine by enchainning growing bacteria. *Nature* **544**, 498–502 (2017).
50. Sturm, A. et al. The cost of virulence: retarded growth of *Salmonella* Typhimurium cells expressing type III secretion system 1. *PLoS Pathog.* **7**, e1002143 (2011).
51. Li, H. et al. The outer mucus layer hosts a distinct intestinal microbial niche. *Nat. Commun.* **6**, 8292 (2015).
52. Apprill, A., McNally, S., Parsons, R. & Weber, L. Minor revision to V4 region SSU rRNA 806R gene primer greatly increases detection of SAR11 bacterioplankton. *Aquatic Microbial Ecol.* **75**, 129–137 (2015).
53. Parada, A. E., Needham, D. M. & Fuhrman, J. A. Every base matters: assessing small subunit rRNA primers for marine microbiomes with mock communities, time series and global field samples. *Environ. Microbiol.* **18**, 1403–1414 (2016).
54. Dey, N. et al. Regulators of gut motility revealed by a gnotobiotic model of diet–microbiome interactions related to travel. *Cell* **163**, 95–107 (2015).
55. Fuhrer, T., Heer, D., Begemann, B. & Zamboni, N. High-throughput, accurate mass metabolome profiling of cellular extracts by flow injection-time-of-flight mass spectrometry. *Anal. Chem.* **83**, 7074–7080 (2011).
56. Kanehisa, M. & Goto, S. KEGG: Kyoto Encyclopedia of Genes and Genomes. *Nucleic Acids Res.* **28**, 27–30 (2000).
57. Yin, S. et al. Factors affecting separation and detection of bile acids by liquid chromatography coupled with mass spectrometry in negative mode. *Anal. Bioanal. Chem.* **409**, 5533–5545 (2017).
58. Wiegand, I., Hilpert, K. & Hancock, R. E. Agar and broth dilution methods to determine the minimal inhibitory concentration (MIC) of antimicrobial substances. *Nat. Protoc.* **3**, 163–175 (2008).
59. Lambert, R. J. & Pearson, J. Susceptibility testing: accurate and reproducible minimum inhibitory concentration (MIC) and non-inhibitory concentration (NIC) values. *J. Appl. Microbiol.* **88**, 784–790 (2000).
60. Cremer, J., Arnoldini, M. & Hwa, T. Effect of water flow and chemical environment on microbiota growth and composition in the human colon. *Proc. Natl Acad. Sci. USA* **114**, 6438–6443 (2017).
61. Vandeputte, D. et al. Quantitative microbiome profiling links gut community variation to microbial load. *Nature* **551**, 507–511 (2017).
62. Soetaert, K., Petzoldt, T. & Setzer, R. W. Solving differential equations in R: Package deSolve. *J. Stat. Softw.* **33**, 1–25 (2010).
63. R Core Team R. *A Language and Environment for Statistical Computing* (R Foundation for Statistical Computing, 2014); <https://www.R-project.org/>
64. Letunic, I. & Bork, P. Interactive tree of life (iTOL) v3: an online tool for the display and annotation of phylogenetic and other trees. *Nucleic Acids Res.* **44**, W242–W245 (2016).

Acknowledgements

We thank members of the Hardt laboratory and R. Stocker for helpful scientific discussions and the RCHCI staff (especially K. Holzinger, D. Mollenhauer and S. Nowok) for excellent support of our animal work. E.S. is supported by the Swiss National Science Foundation (SNF, Marie Heim-Vögtlin award PMPDP3_158364 and Ambizione award PZ00P3_136742) and the Gebert Rief 'Microbials' programme (GRS-073/17). W.-D.H. is supported by the SNF (310030_153074 and 310030B_173338/1; Sinergia CRSII_154414/1; NRP 72 407240-167121), ETH Zurich (ETH-33 12-2), the Novartis Freenovation Programme and the Promedica Foundation. S.S. is supported by ETH Zurich and the Helmut Horten Foundation. E.B. is supported by a Boehringer Ingelheim Fonds PhD Stipend and E.G. by a grant from the Monique Dornonville de la Cour Foundation. B.S. is supported by the German Research Foundation (STE 1971/4-2 SPP 1656/2) and the German Center for Infection Research (DZIF).

Author contributions

S.Y.W. contributed to Figs. 1–3 and Supplementary Figs. 2–5, 7, 8, 10, 11, 16, 18, 22 and 23, B.N. to Supplementary Fig. 24, L.M. and A.T. to Fig. 2e and Supplementary Fig. 12, A.O.B. and J.P. to Fig. 2a, M.A. to Fig. 3a,b and Supplementary Figs. 13–15, D.L.B. to Supplementary Figs. 19 and 21b and Supplementary Tables 4 and 5, M. Zünd and S.S. to Supplementary Figs. 7 and 26, A.H. to Supplementary Fig. 21, E.B. and M.D. to Fig. 1e and Supplementary Fig. 6, K.M. to Fig. 1b–d, M.K. to Fig. 4 and Supplementary Figs. 4, 17, 18g and 25, D.H. and E.S. to Fig. 2d and Supplementary Fig. 23, M.B. and B.S. to Supplementary Fig. 7b, T.D. to Supplementary Fig. 19, M. Zimmermann, T.F. and U.S. to Supplementary Figs. 9 and 18a–b,f and E.G. to Supplementary Fig. 20. A.J.M. and B.S. (Oligo mice) performed the experiments and analysed the data. S.Y.W., M.K., B.N., L.M., D.H., E.S. and W.-D.H. designed the experiments. S.Y.W., M.K. and W.-D.H. wrote the manuscript.

Competing interests

The authors declare no competing interests.

Additional information

Supplementary information is available for this paper at <https://doi.org/10.1038/s41564-019-0568-5>.

Correspondence and requests for materials should be addressed to W.-D.H.

Reprints and permissions information is available at www.nature.com/reprints.

Publisher's note Springer Nature remains neutral with regard to jurisdictional claims in published maps and institutional affiliations.

© The Author(s), under exclusive licence to Springer Nature Limited 2019

Reporting Summary

Nature Research wishes to improve the reproducibility of the work that we publish. This form provides structure for consistency and transparency in reporting. For further information on Nature Research policies, see [Authors & Referees](#) and the [Editorial Policy Checklist](#).

Statistics

For all statistical analyses, confirm that the following items are present in the figure legend, table legend, main text, or Methods section.

n/a Confirmed

- | | | |
|-------------------------------------|-------------------------------------|--|
| <input type="checkbox"/> | <input checked="" type="checkbox"/> | The exact sample size (n) for each experimental group/condition, given as a discrete number and unit of measurement |
| <input type="checkbox"/> | <input checked="" type="checkbox"/> | A statement on whether measurements were taken from distinct samples or whether the same sample was measured repeatedly |
| <input type="checkbox"/> | <input checked="" type="checkbox"/> | The statistical test(s) used AND whether they are one- or two-sided
<i>Only common tests should be described solely by name; describe more complex techniques in the Methods section.</i> |
| <input type="checkbox"/> | <input checked="" type="checkbox"/> | A description of all covariates tested |
| <input type="checkbox"/> | <input checked="" type="checkbox"/> | A description of any assumptions or corrections, such as tests of normality and adjustment for multiple comparisons |
| <input type="checkbox"/> | <input checked="" type="checkbox"/> | A full description of the statistical parameters including central tendency (e.g. means) or other basic estimates (e.g. regression coefficient) AND variation (e.g. standard deviation) or associated estimates of uncertainty (e.g. confidence intervals) |
| <input type="checkbox"/> | <input checked="" type="checkbox"/> | For null hypothesis testing, the test statistic (e.g. F , t , r) with confidence intervals, effect sizes, degrees of freedom and P value noted
<i>Give P values as exact values whenever suitable.</i> |
| <input checked="" type="checkbox"/> | <input type="checkbox"/> | For Bayesian analysis, information on the choice of priors and Markov chain Monte Carlo settings |
| <input checked="" type="checkbox"/> | <input type="checkbox"/> | For hierarchical and complex designs, identification of the appropriate level for tests and full reporting of outcomes |
| <input checked="" type="checkbox"/> | <input type="checkbox"/> | Estimates of effect sizes (e.g. Cohen's d , Pearson's r), indicating how they were calculated |

Our web collection on [statistics for biologists](#) contains articles on many of the points above.

Software and code

Policy information about [availability of computer code](#)

Data collection

The mathematical model is described in detail in the supplementary materials section.

Data analysis

All statistical analysis software is described in the Materials and Methods.

For manuscripts utilizing custom algorithms or software that are central to the research but not yet described in published literature, software must be made available to editors/reviewers. We strongly encourage code deposition in a community repository (e.g. GitHub). See the Nature Research [guidelines for submitting code & software](#) for further information.

Data

Policy information about [availability of data](#)

All manuscripts must include a [data availability statement](#). This statement should provide the following information, where applicable:

- Accession codes, unique identifiers, or web links for publicly available datasets
- A list of figures that have associated raw data
- A description of any restrictions on data availability

All data needed to evaluate the conclusions in this Article are presented in the paper or the Supplementary Information. Any additional data can be requested from the corresponding author.

Field-specific reporting

Please select the one below that is the best fit for your research. If you are not sure, read the appropriate sections before making your selection.

- Life sciences Behavioural & social sciences Ecological, evolutionary & environmental sciences

Life sciences study design

All studies must disclose on these points even when the disclosure is negative.

Sample size	Sample size was determined from data of previous studies.
Data exclusions	We did not exclude any data.
Replication	Biological and/or technical replicates were performed for all experiments and confirmed reproducible.
Randomization	Simple/block randomization was used to allocate animals to experimental and control groups. Groups were age and sex matched as described.
Blinding	Scientists were not blinded for the assignment of the experiments and data analysis.

Reporting for specific materials, systems and methods

We require information from authors about some types of materials, experimental systems and methods used in many studies. Here, indicate whether each material, system or method listed is relevant to your study. If you are not sure if a list item applies to your research, read the appropriate section before selecting a response.

Materials & experimental systems

n/a	Included in the study
<input checked="" type="checkbox"/>	<input type="checkbox"/> Antibodies
<input checked="" type="checkbox"/>	<input type="checkbox"/> Eukaryotic cell lines
<input checked="" type="checkbox"/>	<input type="checkbox"/> Palaeontology
<input type="checkbox"/>	<input checked="" type="checkbox"/> Animals and other organisms
<input checked="" type="checkbox"/>	<input type="checkbox"/> Human research participants
<input checked="" type="checkbox"/>	<input type="checkbox"/> Clinical data

Methods

n/a	Included in the study
<input checked="" type="checkbox"/>	<input type="checkbox"/> ChIP-seq
<input type="checkbox"/>	<input checked="" type="checkbox"/> Flow cytometry
<input checked="" type="checkbox"/>	<input type="checkbox"/> MRI-based neuroimaging

Animals and other organisms

Policy information about [studies involving animals](#); [ARRIVE guidelines](#) recommended for reporting animal research

Laboratory animals	Male and female 8-to-12-week-old mice (C57BL/6 and 129 SvEV) were used in this study. Full husbandry and experimental details are provided in Materials and Methods.
Wild animals	Study did not involve wild animals
Field-collected samples	Study did not involve samples collected from the field
Ethics oversight	All animal experiments were reviewed and approved by the Kantonales Veterinäräm, Zürich (license 222/2013 + 193/2016) and are subject to the Swiss animal protection law (TschG)

Note that full information on the approval of the study protocol must also be provided in the manuscript.

Flow Cytometry

Plots

Confirm that:

- The axis labels state the marker and fluorochrome used (e.g. CD4-FITC).
- The axis scales are clearly visible. Include numbers along axes only for bottom left plot of group (a 'group' is an analysis of identical markers).
- All plots are contour plots with outliers or pseudocolor plots.
- A numerical value for number of cells or percentage (with statistics) is provided.

Methodology

Sample preparation	See Materials and Methods for detailed sample preparation protocols.
Instrument	LSRII Flow cytometer (Becton Dickinson, NJ, USA)

Software	<input type="text" value="FlowJo software 10.4.2 (Treestar, Ashland, OR, USA), FACSDiva (BD Biosciences)"/>
Cell population abundance	<input type="text" value="See exemplary graphs in the manuscript."/>
Gating strategy	<input type="text" value="See gating strategies in the manuscript."/>

Tick this box to confirm that a figure exemplifying the gating strategy is provided in the Supplementary Information.